Liquid metal slingshot

Zhiping Yuan,[1] Xudong Zhang,[2] Huimin Hou,[1] Zhifeng Hu,[1]
Xiaomin Wu ®,[1,*,†] and Jing Liu ®[2,3,*,‡]

[1]*Key Laboratory for Thermal Science and Power Engineering of Ministry of Education,
Department of Energy and Power Engineering, Tsinghua University, Beijing 100084, China*
[2]*Key Lab of Cryogenics, Technical Institute of Physics and Chemistry,
Chinese Academy of Sciences, Beijing 100190, China*
[3]*Department of Biomedical Engineering, School of Medicine, Tsinghua University, Beijing 100084, China*

This Rapid Communication presents the self-propelled and controllable motion of liquid metal droplets, which is driven by surface tension and does not depend on any external force field. Its motion speed and direction can be controlled just as a projectile fired by a slingshot: The liquid metal droplet is the projectile, and a substrate surface serves as the bowstring. This motion provides a potential mechanism for the application of liquid metals in soft robotics, drug delivery, chip cooling, and other fields.

Liquid metal is of core interest for a wide variety of newly emerging areas, such as enhanced cooling [1–3], drug delivery [4,5], soft robotics [6–10], deformable metal material [11–13], and microfluidic chip [14–16], because of its excellent conductivity, thermal conductivity, biocompatibility, favorable flexibility, and fluidity. The essential aspect of these applications is the motion of liquid metal droplets, which is typically triggered by external fields, such as the magnetic field [14,17] and electricity [18,19]. Although these driving mechanisms are well understood, these motion processes are not self-propelled, which limits the application potential of liquid metal.

Surface tension can drive aqueous liquids to produce a series of self-propelled motion phenomena. For instance, the directional transport of droplets occurs on a surface with a wetting gradient or with an anisotropic structure [20–23], the self-propelled jumping and sweeping of condensing droplets on the superhydrophobic surface [24–27], and the rotation or curling of an ice water mixture on a superhydrophobic surface or a slippery surface [28,29]. These self-propelled motions have a high scientific and application value and are still the research hotspots at present. The surface tension coefficient of liquid metal is higher than that of aqueous liquids, and its dynamic viscosity is lower than that of aqueous liquids. The effect of surface tension should be more significant, and the surface tension may replace the electric force and magnetic force as the driving force in the micro- and nanoscale. In contrast with the current popular research on the self-propelled motion of aqueous liquids, the research on self-propelled of liquid metals needs more attention.

In this Rapid Communication, a self-propelled and controllable motion of liquid metal droplets is reported. Liquid metal droplets can move independent of the external force field, and can optionally change the projection direction and velocity by changing the shape of the bowstring (substrate surface). Combined with experiments and simulation, the firing mechanism is analyzed, and a

---

*These authors contributed equally to this work.
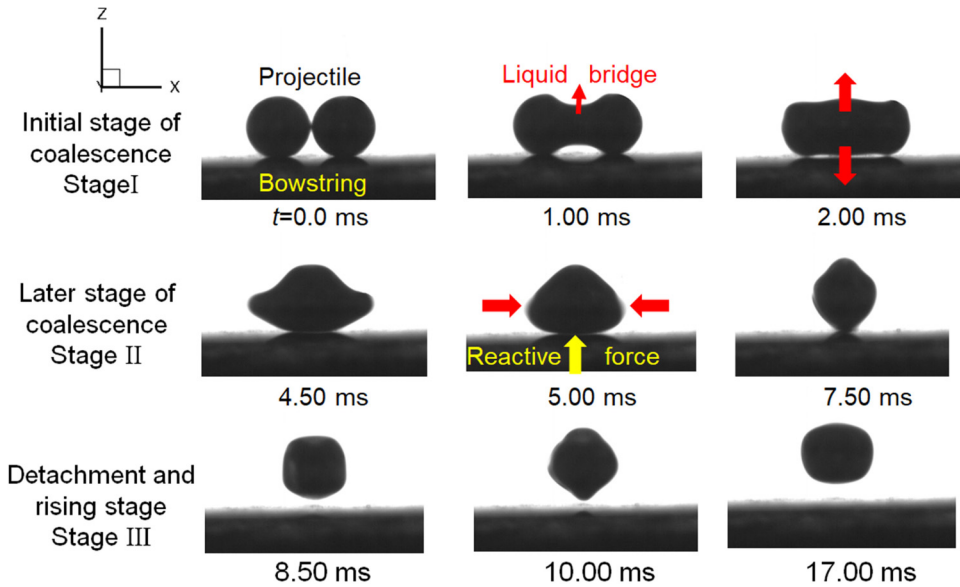†wuxiaomin@mail.tsinghua.edu.cn
‡jliu@mail.ipc.ac.cn

FIG. 1. The morphology evolution of a liquid metal droplet with time in case 1. The volume of a single droplet is 2.5 μl, and the radius is 842 μm. The velocity of the droplets when they depart the surface is about 0.160 m/s. Two groups of red arrows in the figure respectively indicate the expansion of the liquid bridge and the contraction of the droplets.

theoretical model of the relationship between the projection velocity, direction, and bowstring shape is established.

The liquid metal used in this Rapid Communication is a gallium indium alloy (weight percentage, Ga 90%, In 10%, 6280 kg/m^3) with a high surface tension (0.65 N/m) and low viscosity (2.7×10^{-7} m^2/s) [30]. Two liquid metal droplets of a suitable size are produced by a microsyringe on the substrate surface, and then the two droplets are gently stirred to coalesce and fire. In order to prevent the oxide layer on the liquid metal surface from blocking the flow of the liquid metal, the experiments are carried out in a 0.5 mol/ℓ NaOH solution. The materials of the substrate surface used in the experiments include a silicon wafer, glass, and an aluminum surface modified by 1H,1H,2H,2H-perfluorodecyltriethoxysilane (Al-FAS). The purpose of using FAS to modify the aluminum surface is to prevent the double electric layer from blocking the coalescence of the droplets and also delaying the reaction between Al and NaOH. In the modification step, the aluminum surface is polished with 1000-grit sandpaper, then placed in a 0.1 mol/ℓ FAS solution for 30 min, and then dried in an oven at 100 °C for 30 min. The contact angle of liquid metal droplets on Al-FAS, glass, and the silicon wafer substrate surface is about 140°–150°. The simulation uses the INTERFOAM solver based on the volume of fluid (VOF) in OPENFOAM. The size of the simulation domain is 6 mm × 6 mm × 6 mm, and the mesh resolution is 200 × 200 × 200. The substrate surface is set as the superhydrophobic nonslip boundary condition, and the other is the pressure outlet boundary condition. The physical parameters are the same as the experimental parameters. More detailed experiments and simulations can be seen in our previous research [16,26,31].

Figure 1 shows the coalescence of two liquid metal droplets on the Al-FAS substrate (case 1, see Movie S1 in the Supplemental Material [32]). At the initial stage of coalescence (stage I), a liquid bridge (0.0–1.00 ms) is generated at the contact position of the two droplets. Then, the liquid bridge expands under the surface tension and finally contacts the substrate (1.00–2.00 ms). At the later stage of coalescence (stage II), the liquid bridge expands further, and the droplets begin to contract towards the middle. The reaction force of the substrate surface to the liquid bridge makes

the droplets depart from the substrate surface (4.00–8.50 ms). After the droplet departs off the surface, it rises with deformation (8.50–17.00 ms).

At the initial impression, the experimental results in Fig. 1 will cause confusion because we do not think that energy is stored on a straight bowstring in general, and then a straight bowstring cannot fire the projectile. The energy stored by the bowstring in the liquid metal slingshot is the surface energy, while that of the ordinary slingshot is the elastic potential energy. This difference can be revealed by analyzing the energy change of the liquid metal slingshot. We use a simulation to study the process of energy conversion because it is difficult to measure in the experiment. The change in projection kinetic energy ΔE_k from the initial state is calculated as follows,

$$\Delta E_k = \tfrac{1}{2}m(u^2 + v^2 + w^2),\tag{1}$$

where m is the mass of the droplet, and u, v, and w are the average mass velocities in the X, Y, and Z directions, respectively. The change of surface energy consists of three parts: the change of surface energy of the liquid metal-NaOH solution interface ΔE_{ml}, the change of surface energy of the liquid metal-substrate interface ΔE_{ms}, and the change of surface energy of the substrate interface-NaOH solution ΔE_{sl}, respectively. The surface energy change is equal to the product of the change of surface area and the coefficient of surface tension,

$$\begin{aligned}\Delta E_s &= \Delta E_{ml} + \Delta E_{ms} + \Delta E_{sl}\\ &\Rightarrow \delta_{ml}\Delta A_{ml} + \delta_{ms}\Delta A_{ms} + \delta_{sl}\Delta A_{sl},\end{aligned}\tag{2}$$

where δ and ΔA are the surface tension coefficient and area change of three interfaces. The area change values of the metal-substrate interface and solution-substrate interface are equal, $\Delta A_{ms} = -\Delta A_{ml}$, and these two energy changes are marked as ΔE_{msl} together. According to Young's equation, Eq. (2) can be written as follows,

$$\Delta E_s = \delta_{ml}\Delta A_{ml} - \delta_{ml}\cos(\theta)\Delta A_{ms},\tag{3}$$

where θ is the contact angle. ΔA_{ml} of two small globular droplets coalescing into a big globular droplet can be defined as

$$\Delta A_{ml} = -4\pi R^2\left[1 - \cos(\theta) - \left(\frac{[\cos(\theta) - 1]^2[\cos(\theta) + 2]}{2}\right)\right]^{2/3} + O,\tag{4}$$

where R is the initial droplet radius, and O is a small quantity. ΔA_{ms} can be defined as

$$\begin{aligned}\Delta A_{ms} = \frac{4R^2\sin(\theta)}{\sin(\theta_{bb})}&\left[\sin(\theta_{bb})\sin(\theta)\arccos\left(\frac{\cos(\theta_{bb})\cos(\theta)}{\sin(\theta_{bb})\sin\theta}\right)\right.\\ &\left.- \cos(\theta_{bb})\cos(\theta)\left(\frac{\sin(\theta)^2 + \sin(\theta_{bb}/2)^2 - 1}{\sin(\theta_{bb})^2\sin(\theta)^2}\right)^{1/2}\right],\end{aligned}\tag{5}$$

where θ_{bb} is half the angle between the two bowstrings, and the contact angle is taken as the median value 145° of the contact angle of three surfaces. See Supplemental Material for the detailed derivation [32]. Figure 2 shows the surface energy and projection kinetic energy of case1 in Fig. 1 as a function of time. E_{ml} decreases at the initial stage of coalescence (stage I) and increases slightly at the stage of contraction and detachment (stage II). For E_{msl}, the generation and expansion of the liquid metal bridge make the metal fluid concentrate in the middle, and the contact surface between the liquid metal and substrate decreases until the liquid metal bridge contacts the substrate surface, first resulting in its decrease, and then an increase (stage I). Then, E_{msl} decreases with the droplet shrinking (stage II). The projection kinetic energy of liquid metal droplets hardly changes in stage I, but increases rapidly in stage II, and decreases dramatically before departing the substrate. When the droplet departs off the surface, that is, the beginning of stage III, the surface energy E_{msl} can be released entirely. In contrast, the surface energy of the liquid metal solution cannot be released entirely due to the large deformation of the droplet, which is only about 60% of the ideal release
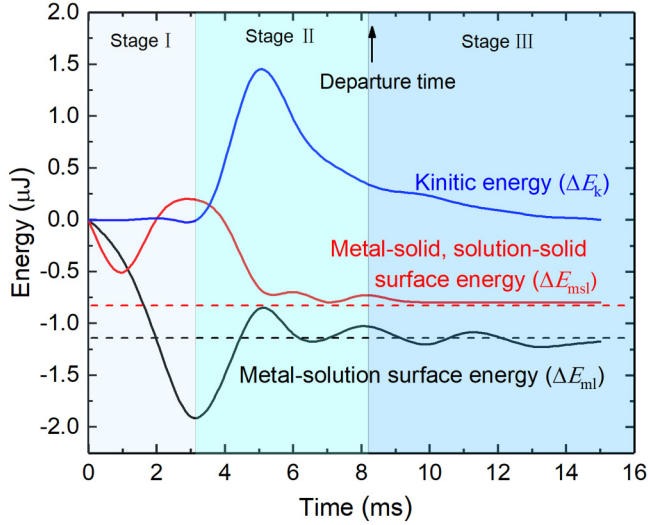
FIG. 2. Variation of surface energy and projection kinetic energy vs time. The dotted lines in red and black are the theoretical values from Eqs. (4) and (5), respectively. The simulated results are very close to the theoretical results.

amount [Eq. (4)], and the effective release amount of E_{ml} is almost the same as the release amount of E_{msl}.

Figure 3 shows the change of projection velocity of the liquid metal droplet on three straight substrates of Al-FAS, silicon wafer, and glass with a droplet radius, respectively. We can see that the projection velocity of the liquid metal droplets decreases with an increase of radius and is not affected by the substrate materials. According to the dimensionless processing methods of impact, rebound, and coalescence of a water droplet in past studies, the dimensionless processing of projection velocity is defined as [33–35]

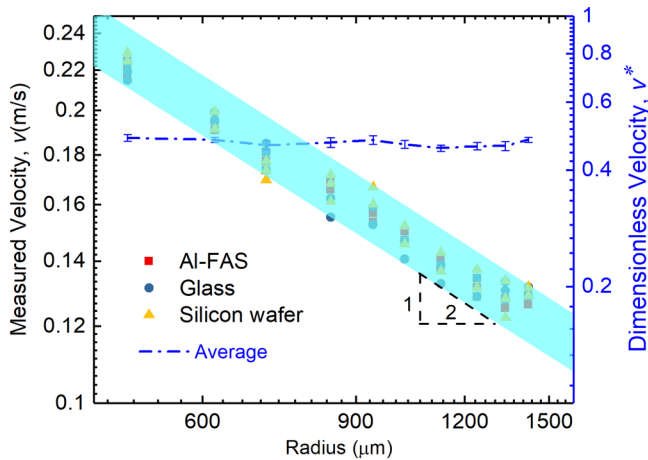$$v^* = v/(\delta_{ml}/\rho R)^{1/2}, \tag{6}$$

FIG. 3. Variation of projection velocity and dimensionless velocity with droplet radius. All data are from the experiment. The dotted line average representatives the average values of dimensionless velocities on different substrate surfaces
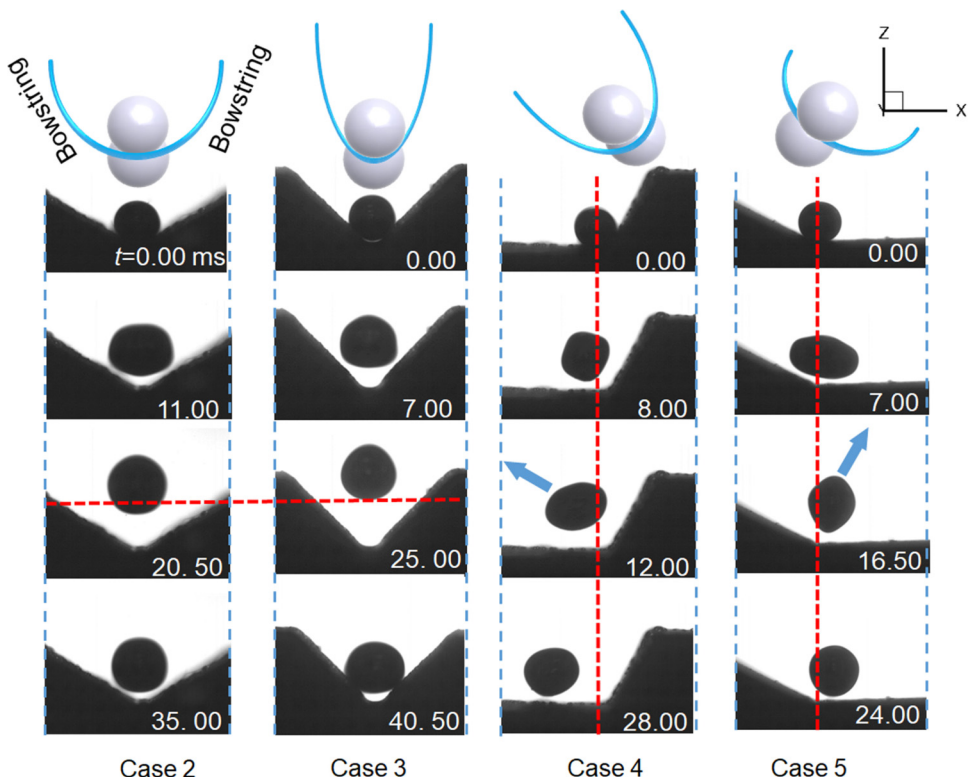
FIG. 4. The effect of bowstring shape on projection velocity and direction. Two equal-sized liquid metal droplets are placed back and forth to coalesce and induce the firing. The angle between the two bowstrings in case 2 and case 3 is 120° and 90°, and the bisector of the two bowstrings is perpendicular to the substrate. The angle between the two bowstrings in case 4 and case 5 is 120° and 150°, and the angle between the bisector and the substrate is 120° and 60°.

where ρ is the density of the liquid metal, and v and v^* are the measured velocity and the dimensionless velocity, respectively. As shown in Fig. 3, for the projection of two equal liquid metal droplets, the dimensionless projection velocity is almost independent of the droplet radius and substrate materials. According to this, we can define the projection velocity of the liquid metal projectile as

$$v = C_0(\delta_{\mathrm{ml}}/\rho R)^{1/2}, \tag{7}$$

so when the shape of the bowstring is straight, C_0 is 0.45–0.48. We compared the velocity with the water droplet in the Supplemental Material [32].

Figure 4 shows how to control the projection velocity and direction by changing the shape of the bowstring (see Movies S2–S5 [32]). When the bowstring is stretched (case 1→case 5→case 2, case 4→case 3), the projection velocity increases when the bowstring deformation increases, thus the maximum projection height increases, and the stagnation time after departure increases. By changing the angle of the bowstring (case 1, case 2, case 3→case 4→case 5), the liquid metal projectile can be propelled in the expected direction.

Figure 5(a) shows the relationship between the amount of surface energy stored by the bowstring and the shape of the bowstring. The angle between the two bowstrings changes from 180° in case 1 to 90° in case 3, and the contact point between the single liquid metal droplet and the substrate changes from one to two. Thus both the contact area and the energy stored by the bowstring are
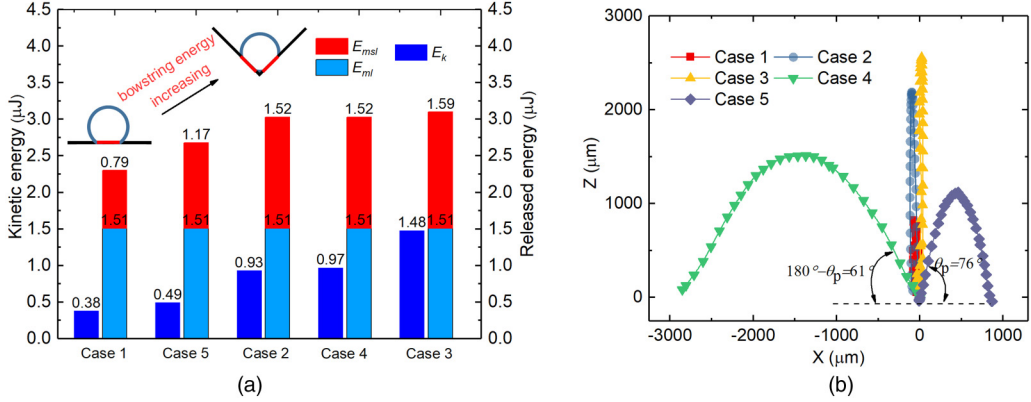
FIG. 5. (a) The relationship between projection kinetic energy, bowstring energy, and bowstring shape. The calculation of kinetic energy takes the average projection velocity of three experiments for each case. (b) The relationship between the projection direction and the shape of the bowstring. Case 1 is the case shown in Fig. 1. The radii of droplets are 842 μm in all cases and the substrate material is Al-FAS.

doubled. For case 5, case 2, and case 4, the surface energy and projection kinetic energy also increase with the elongation of the bowstring. In addition, the elongation of the bowstring increases the ratio of the released surface energy to the projection kinetic energy, and then increases the projection velocity. The values of C_0 in Eq. (5) corresponding to the bowstring angles of 180°, 150°, 120°, and 90° are 0.47, 0.55, 0.73, and 0.90. Liquid metal droplets fire under the reaction force of the bowstring, so changing the bowstring shape can control the projection direction. Assuming that the components of the force exerted by a single bowstring on the liquid metal in the horizontal and vertical directions are $F \sin(\theta_b)$ and $F \cos(\theta_b)$, where θ_b is the angle between the bowstring and the horizontal direction, the direction of the resultant force of the two bowstrings is

$$\theta_p = arctan\left(\frac{\cos(\theta_{b1}) + \cos(\theta_{b2})}{\sin(\theta_{b1}) - \sin(\theta_{b2})}\right), \quad (8)$$

where θ_p is the projection direction, and θ_{b1} and θ_{b2} are the angles between the two bowstrings and the horizontal direction. As shown in Fig. 5(b), the theoretical projection directions of cases 1–5 are 90°, 90°, 90°, 120°, and 75°, respectively, and the experimental and theoretical results are consistent.

In summary, we report the self-propelled motion of liquid metal droplets, and its projection velocity and direction changing with the shape of the bowstring as a slingshot. We examine the firing mechanism with experiments and a numerical simulation and then establish a theoretical model to reveal the relationship between the projection velocity, direction, and bowstring shape. This self-propelled motion, and our research on it, has enriched the study of liquid metals. In particular, the projection velocity and direction can be easily controlled by the bowstring, which suggests a potential means for soft robotics, drug delivery, and others.

The firing of liquid metal droplets is very similar in form to the self-propelled jumping of aqueous droplets in that both are induced by coalescence. However, the jumping of aqueous droplets cannot occur on the common materials used in this Rapid Communication, but only on expensive and nondurable superhydrophobic surfaces. For the control of velocity and direction, there is a lack of similar studies on aqueous droplets for comparison. In addition, the application of liquid metal is

quite different from that of water because of its excellent fluidity, conductivity, thermal conductivity, and biocompatibility.

---

[1] K. Ma and J. Liu, Liquid metal cooling in thermal management of computer chips, Front. Energy Power Eng. China **1**, 384 (2007).

[2] G. Bo, L. Ren, X. Xu, Y. Du, and S. Dou, Recent progress on liquid metals and their applications, Adv. Phys.: X **3**, 1446359 (2018).

[3] T. Foulkes, S. Sett, P. Sokalski, J. Oh, and N. Miljkovic, Fundamental limits of jumping droplet heat transfer, Appl. Phys. Lett. **116**, 093701 (2020).

[4] C. A. R. Chapman, E. A. Cuttaz, J. A. Goding, and R. A. Green, Actively controlled local drug delivery using conductive polymer-based devices, Appl. Phys. Lett. **116**, 010501 (2020).

[5] V. T. Dau, T.-K. Nguyen, and D. V. Dao, Charge reduced nanoparticles by sub-kHz ac electrohydrodynamic atomization toward drug delivery applications, Appl. Phys. Lett. **116**, 023703 (2020).

[6] D. Wang, C. Gao, W. Wang, M. Sun, B. Guo, H. Xie, and Q. He, Shape-transformable, fusible rodlike swimming liquid metal nanomachine, ACS Nano **12**, 10212 (2018).

[7] Y. Yu and E. Miyako, Recent advances in liquid metal manipulation toward soft robotics and biotechnologies, Chem. Eur. J. **24**, 9456 (2018).

[8] J. Zhang, R. Guo, and J. Liu, Self-propelled liquid metal motors steered by a magnetic or electrical field for drug delivery, J. Mater. Chem. B **4**, 5349 (2016).

[9] Y. Yang, N. Sun, Z. Wen, P. Cheng, H. Zheng, H. Shao, Y. Xia, C. Chen, H. Lan, X. Xie, C. Zhou, J. Zhong, X. Sun, and S.-T. Lee, Liquid-metal-based super-stretchable and structure-designable triboelectric nanogenerator for wearable electronics, ACS Nano **12**, 2027 (2018).

[10] J. Zhang, Y. Yao, L. Sheng, and J. Liu, Self-fueled biomimetic liquid metal mollusk, Adv. Mater. **27**, 2648 (2015).

[11] B. Yuan, C. Zhao, X. Sun, and J. Liu, Liquid-metal-enhanced wire mesh as a stiffness variable material for making soft robotics, Adv. Eng. Mater. **21**, 1900530 (2019).

[12] Y. Hou, H. Chang, K. Song, C. Lu, P. Zhang, Y. Wang, Q. Wang, W. Rao, and J. Liu, Coloration of liquid-metal soft robots: from silver-white to iridescent, ACS Appl. Mater. Interfaces **10**, 41627 (2018).

[13] S. Liang, W. Rao, K. Song, and J. Liu, Fluorescent liquid metal as a transformable biomimetic chameleon, ACS Appl. Mater. Interfaces **10**, 1589 (2018).

[14] L. Hu, L. Wang, Y. Ding, S. Zhan, and J. Liu, Manipulation of liquid metals on a graphite surface, Adv Mater. **28**, 9210 (2016).

[15] M. G. Pollack, R. B. Fair, and A. D. Shenderov, Electrowetting-based actuation of liquid droplets for microfluidic applications, Appl. Phys. Lett. **77**, 1725 (2000).

[16] X. Zhao, S. Xu, and J. Liu, Surface tension of liquid metal: Role, mechanism and application, Front. Energy **11**, 535 (2017).

[17] L. Hu, H. Wang, X. Wang, X. Liu, J. Guo, and J. Liu, Magnetic liquid metals manipulated in the three-dimensional free space, ACS Appl. Mater. Interfaces **11**, 8685 (2019).

[18] S. W. Jin, Y. R. Jeong, H. Park, K. Keum, G. Lee, Y. H. Lee, H. Lee, M. S. Kim, and J. S. Ha, A flexible loudspeaker using the movement of liquid metal induced by electrochemically controlled interfacial tension, Small **15**, 1905263 (2019).

[19] M. F. Wang, M. J. Jin, X. J. Jin, and S. G. Zuo, Modeling of movement of liquid metal droplets driven by an electric field, Phys. Chem. Chem. Phys. **19**, 18505 (2017).

[20] H. Chen, T. Ran, Y. Gan, J. Zhou, Y. Zhang, L. Zhang, D. Zhang, and L. Jiang, Ultrafast water harvesting and transport in hierarchical microchannels, Nat. Mater. **17**, 935 (2018).

[21] J. Ju, Y. Zheng, and L. Jiang, Bioinspired one-dimensional materials for directional liquid transport, Acc. Chem. Res. **47**, 2342 (2014).

[22] M. Zhang and Y. Zheng, Bioinspired structure materials to control water-collecting properties, Mater. Today: Proc. **3**, 696 (2016).

[23] G. Zhu, J. Kou, B. Yao, Y.-S. Wu, J. Yao, and S. Sun, Thermodynamically consistent modelling of two-phase flows with moving contact line and soluble surfactants, J. Fluid Mech. **879**, 327 (2019).

[24] Z. Yuan, R. Wu, and X. M. Wu, Numerical simulations of multi-hop jumping on superhydrophobic surfaces, Int. J. Heat Mass Transfer **135**, 345 (2019).

[25] X. Yan, L. Zhang, S. Sett, L. Feng, C. Zhao, Z. Huang, H. Vahabi, A. K. Kota, F. Chen, and N. Miljkovic, Droplet jumping: effects of droplet size, surface structure, pinning, and liquid properties, ACS Nano **13**, 1309 (2019).

[26] Z. Yuan, Z. Hu, F. Chu, and X. M. Wu, Enhanced and guided self-propelled jumping on the superhydrophobic surfaces with macrotexture, Appl. Phys. Lett. **115**, 163701 (2019).

[27] X. Qu, J. B. Boreyko, F. Liu, R. L. Agapov, N. V. Lavrik, S. T. Retterer, J. J. Feng, C. P. Collier, and C. Chen, Self-propelled sweeping removal of dropwise condensate, Appl. Phys. Lett. **106**, 221601 (2015).

[28] F. Chu, X. M. Wu, and L. Wang, Dynamic melting of freezing droplets on ultraslippery superhydrophobic surfaces, ACS Appl. Mater. Interfaces **9**, 8420 (2017).

[29] F. Chu, X. M. Wu, and L. Wang, Meltwater evolution during defrosting on superhydrophobic surfaces, ACS Appl. Mater. Interfaces **10**, 1415 (2018).

[30] Y. Plevachuk, V. Sklyarchuk, S. Eckert, G. Gerbeth, and R. Novakovic, Thermophysical properties of the liquid Ga-In-Sn eutectic alloy, J. Chem. Eng. Data **59**, 757 (2014).

[31] R. Guo, X. Sun, B. Yuan, H. Wang, and J. Liu, Magnetic liquid metal (Fe-EGaIn) based multifunctional electronics for remote self-healing materials, degradable electronics, and thermal transfer printing, Adv. Sci. **6**, 1901478 (2019).

[32] See Supplemental Material at http://link.aps.org/supplemental/10.1103/PhysRevFluids.5.111601 for supplemental movies and information as described in the main text.

[33] J. Eggers, J. R. Lister, and H. A. Stone, Coalescence of liquid drops, J. Fluid Mech. **401**, 293 (1999).

[34] J. C. Bird, R. Dhiman, H. M. Kwon, and K. K. Varanasi, Reducing the contact time of a bouncing drop, Nature (London) **503**, 385 (2013).

[35] J. B. Boreyko and C. H. Chen, Self-Propelled Dropwise Condensate on Superhydrophobic Surfaces, Phys. Rev. Lett. **103**, 184501 (2009).